Energetic particles stimulating macro-scale zonal flow generation in ion-temperature-gradient turbulence

To cite this article before publication: Yihan Wang *et al* 2025 *Nucl. Fusion* in press https://doi.org/10.1088/1741-4326/ade4db

Energetic Particles Stimulating Macro-scale Zonal Flow Generation in Ion-temperature-gradient Turbulence

Yihan Wang
Laser Fusion Research Center, China Academic of Engineering Physics, Mianyang 621900, China and State Key Lab of Nuclear Physics and Technology, School of Physics, Peking University, Beijing 100871, China

Zhibin Guo*
Institute of Modern Physics, Fudan University, Shanghai 200433, China and State Key Lab of Nuclear Physics and Technology, School of Physics, Peking University, Beijing 100871, China

Zhihong Lin
Department of Physics and Astronomy, University of California, Irvine, California 92697, USA

Abstract

We report a formation mechanism of macro-scale zonal flow (ZF) in ion-temperature-gradient (ITG) turbulence. Through gyro-kinetic simulations, it finds that the guiding centers of the EPs (energetic particles) open a new dynamical coupling regime ($\sim$ a few EP gyro-radius) between the ITG turbulence and the ZF, so that the ITG turbulence produces a substantial global Reynolds' force, which drives the macro-scale ZF. Besides, with the increase of the EP concentration, the ZF driven by a unit of turbulence intensity — the ZF capability — will get enhanced correspondingly. A kinetic analysis reveals that the EP stimulates macro-scale ZF generation by its strong in-phase effect with the ITG velocity fluctuations, which roots at the large diamagnetic drift frequency of the EP's guiding center. We also carry out numerical experiments and show that in the presence of macro-scale ZF, the intensity of the nonlinearly saturated Alfvén eigenmodes would decrease. Thus, it potentially suggests a direct self-organization process of improving the EP confinement in burning plasma.

I. INTRODUCTION

EPs, the key minority, are crucial in maintaining the self-sustained heating of burning plasmas in magnetically confined fusion reactors[1, 2]. To be detained in the fusion devices, the EPs need overcome their anomalous loss induced by macro-scale MHD modes, such as Alfvén eigenmodes (AEs) and internal kink modes, which are in turn driven by the EPs themselves[3, 4]. On the other hand, the EP-heated fusion fuels (background plasmas) are usually subjected to turbulent transport by microscopic instabilities, particularly the ITG mode, and this process constitutes an indirect loss channel of the EP energy. Though ITG turbulence is a major ingredient in lowering the thermal confinement of the background plasmas, it is also a driving force for the plasma self-organizing into a high confinement state, i.e., through ZF generation[5]. Besides linear stabilization effects[6–13], it is reported that the EPs can also nonlinearly regulate the ITG turbulence via the zonal flow generated by macro-scale modes[14–18]. Recently, the zonal flow produced by EP-driven Alfvén modes and its effect in regulating microscopic turbulence have also been reported in tokamak and stellarator experiments[19–21]. This self-organization process can be summarized as follows: EPs initially destabilize AEs. The AEs then drive zonal flow, and suppress the ITG turbulence, improving the confinement of the background plasmas.

In this work, we report that EPs can directly enhance the efficiency of ZF generation in ITG turbulence. By defining a specific ZF capability, which accounts for the ZF intensity generated by a unit of ITG turbulence intensity, it finds that the EPs can increase both the ZF capability and the proportion of macro-scale zonal flow. This effect comes from the strong phase coupling between the EP guiding center density and the ITG fluctuations, independent of the weak coupling between the EP polarization density and the ITG. In spite of the smallness of the amplitude of the EP guiding center fluctuations, its cross-phase with the ITG radial velocity fluctuation is either locked to 0 or π. This in-phase effect produces

* zbguo@pku.edu.cn

a significant EP guiding center flux and hence drives ZF at a length scale of a few EP gyro-radius or at macro-scale. Interestingly, the profile of the cross-phase exhibits resilient property, i.e., persisting from the linear stage to the nonlinear stage, hence it is a robust mechanism for the ZF formation. The macro-scale ZF has prominent effect in suppressing AE modes, through which the EP's confinement is improved, directly.

The remainder of this paper is structured as follows: section 2 outlines the simulation setup and insights from linear and nonlinear simulation results. Section 3 explores the Reynolds' force in describing the zonal flow generation, and investigate the impact of EPs on the zonal flow. Section 4 summarizes our findings.

II. SIMULATION INSIGHTS

We investigate EP's effect on the self-organization physics of ITG turbulence by using the GTC code, in which the ions and EPs are described by their gyro-kinetic equations and electrons by hybrid model of fluid (adiabatic part) and drift-kinetic (non-adiabatic part)[22]. The equilibrium plasma profiles are adopted from DIII-D shot #159243, as shown in Fig. 1(a)-(b). The plasma beta is approximately $\beta = 3.1\%$ on the magnetic axis. Consistent with the reversed q profile (Fig. 1(a)), reversed shear Alfvén eigenmodes (RSAE) is observed in experiment. The EP temperature is approximately 12 times the bulk ion temperature, i.e., $T_{EP} = 24$keV and $T_i = 2$keV on the magnetic axis. For more experimental details, one can refer to[23]. The simulation region is chosen as $r = [0.17, 0.77]a$, with $a = 0.548$m the minor radius. We employ approximately 10^5 grid points in the perpendicular plane in order to capture the short wavelength ITG, and 24 parallel grid points to resolve the long parallel wavelength. The time step is 1.2×10^{-7}s ($\sim 11.4\Omega_{ci}^{-1}$, where $\Omega_{ci} = q_i B_0/M_i$), which is sufficient to resolve the ITG frequency. A periodic boundary condition is employed in the toroidal direction and a linear decay boundary condition is employed in the radial direction.

Electrostatic simulations are initialized using a Maxwellian distribution for all particle species including EP. In our equilibrium, ITG has a toroidal mode number spectrum from $n = 10$ to $n = 25$, with the most unstable branch $n = 16$. To accelerate the simulation and meanwhile not lose the essential nonlinear physics, we keep the $n = 0$ zonal modes and fix the toroidal mode number of the ITG as $n = 16$, and keep all poloidal mode numbers. We have checked that including nonlinear interaction among toroidal mode n does not change our conclusion qualitatively, and it only impacts the quantitative values of each physical quantity. For EP with fixed temperature, the control parameters are its density and density gradient. Here we introduce an EP concentration parameter λ_{EP} to describe its equilibrium profile: $n_{EP} = n_{EP,0} + \lambda_{EP} n_{i,0}$ and $n_i = (1 - \lambda_{EP}) n_{i,0}$, where $n_{EP,0}$ and $n_{i,0}$ correspond to the EP and ion density in the experiment (i.e., $\lambda_{EP} = 0$). The $\eta_i (\equiv \partial_r \ln T_i / \partial_r \ln n_i)$ keeps fixed when increasing λ_{EP}, so that the ITG is mainly impacted by the EP effect. The variation of EP density gradient $R_0/L_{n,EP}$ is shown in Fig. 1(c), along with the ion density gradient (black curve). A scan of the ITG growth rate γ_{ITG} and frequency ω_{ITG} with λ_{EP} is shown in Fig. 1(d), and it is consistent with the well-known result that EP has a linear stabilization effect on ITG mode[7–9, 24].

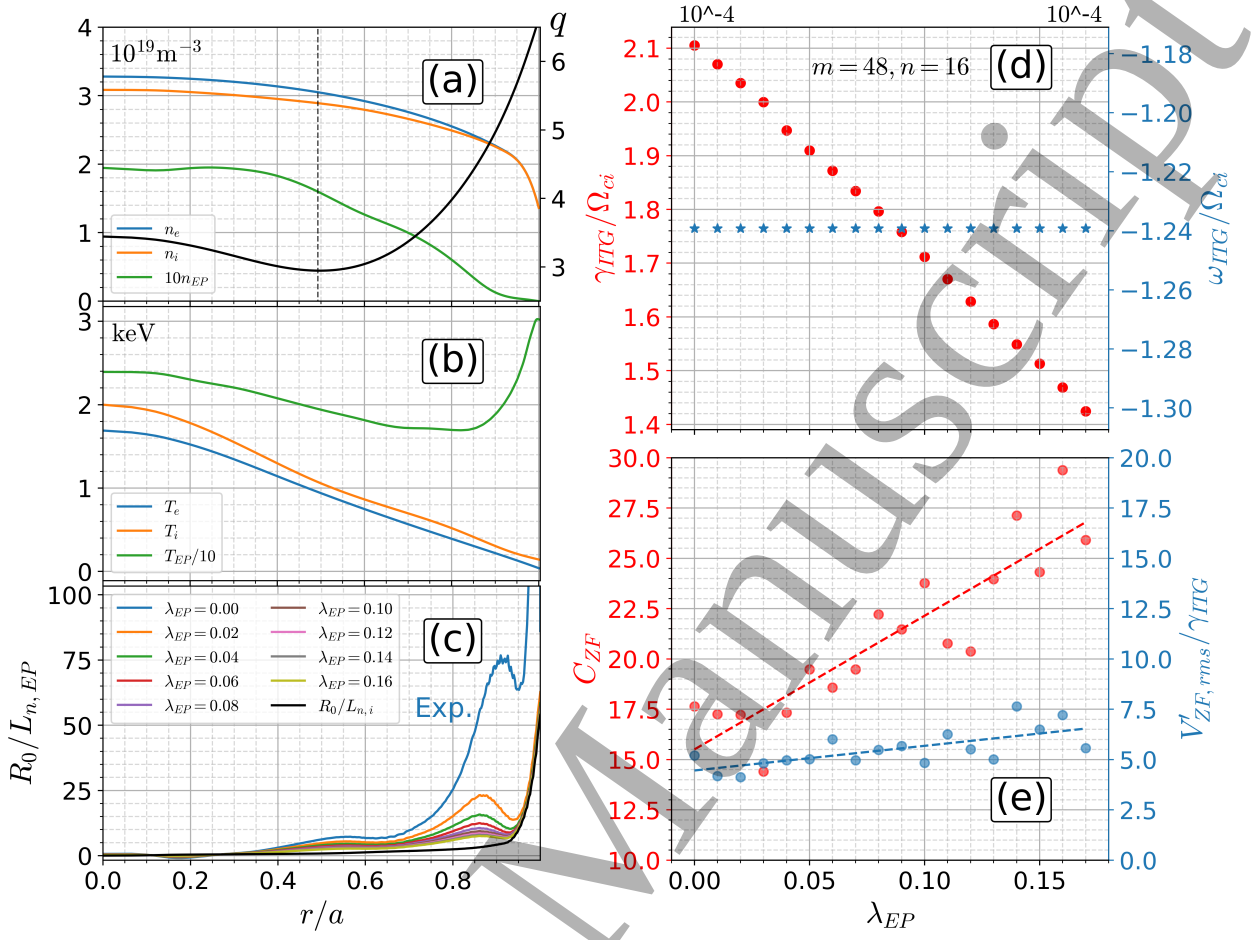

FIG. 1. (a)-(b) Equilibrium density and temperature profiles for the three species with a reversed safety factor profile q. (c) EP density gradient with different λ_{EP} (colored) and ion density gradient (black). (d) Dependence of ITG growth rate γ_{ITG} and frequency ω_{ITG} on λ_{EP}. (e) Dependence of the ZF capability and ZF shearing rate on λ_{EP}.

In the above setup, the increase of λ_{EP} would result in a lower intensity of the saturated ITG turbulence. However, this should not be conceived as a real scenario, because other physical processes may be also happening, e.g., the enhanced EP heating on the background plasmas would increase η_i (γ_{ITG}), and hence it may neutralize λ_{EP}'s stabilization effect. To disentangle the linear impact and extract the nonlinear process of the ITG turbulence, we define a new quantity called 'specific zonal flow capability':

$$C_{ZF} \equiv \frac{V_{ZF,rms}}{\phi^2_{rms}}, \tag{1}$$

where $V_{ZF,rms}$ is the root-mean-square value of the ZF velocity and ϕ^2_{rms} is the fluctuation intensity of electrostatic potential associated with the ITG turbulence. C_{ZF} measures the ability of ZF driving by unit turbulence intensity. As shown in Fig. 1(e), C_{ZF} grows with the increase of λ_{EP}, which implies EP enhances the efficiency of ZF production. While, the

ratio of ZF shear rate V_E' over γ_{ITG} only increases mildly, as is consistent with reduction of γ_{ITG} with the increase of λ_{EP}.

III. ENERGETIC PARTICLES STIMULATING ZONAL FLOW

A. Fluid theory of Reynolds' force

In order to understand how EP changes the ZF capability of the ITG turbulence, we first carry out a fluid analysis. In the fluid model, V_{ZF} is driven by the Reynolds' force: $\mathrm{RF} = -\nabla\cdot\Pi_{r,\theta}$, with $\Pi_{r,\theta} = \langle\tilde{v}_r\tilde{v}_\theta\rangle$ the magnetic surface averaged poloidal velocity flux. For electrostatic fluctuations, we have $\tilde{\boldsymbol{v}} = -\nabla\tilde{\phi}\times\hat{b}/B_0$ and $\tilde{\phi}$ can be expressed as $\tilde{\phi} = \sum_{m,n}\phi_m \mathrm{e}^{-\mathrm{i}m\theta+\mathrm{i}n\zeta}$. The Reynolds' stress then becomes $\Pi_{r,\theta} = (1/B_0^2)\sum_{m>0}\left(-\frac{2m}{r}|\phi_m|^2\partial_r\ln\phi_m\right)$ with n taken fixed. Since $\phi_m = |\phi_m|\mathrm{e}^{\mathrm{i}\Theta_m}$ and $\partial_r\ln\phi_m \to \mathrm{i}\partial_r\Theta_m$, only the phase gradient makes a finite contribution to $\Pi_{r,\theta}$. Correspondingly, the RF is composed of three pieces:

$$\mathrm{RF} = \underbrace{\sum_{m>0}\frac{2m}{rB_0^2}\frac{\partial|\phi_m|^2}{\partial r}\frac{\partial\Theta_m}{\partial r}}_{\mathrm{RF_{amp}}} + \underbrace{\sum_{m>0}\frac{2m}{rB_0^2}|\phi_m|^2\frac{\partial^2\Theta_m}{\partial r^2}}_{\mathrm{RF_{ph}}} + \underbrace{\sum_{m>0}\frac{2m}{r^2B_0^2}|\phi_m|^2\frac{\partial\Theta_m}{\partial r}}_{\mathrm{RF_{geo}}}, \tag{2}$$

where $\mathrm{RF_{amp}}$ is from the gradient of the turbulence intensity, $\mathrm{RF_{ph}}$ is from the phase curvature and $\mathrm{RF_{geo}}$ is the geometric effect. In the experimental case ($\lambda_{EP} = 0$, EP ratio 6%), their spatiotemporal evolutions are plotted in Fig. 2(a-c) and these structures are also consistent with $\partial_t V_{ZF}$. As can be seen, the phase curvature is the dominant RF. The phase-amplitude decomposition of ϕ_m indicates phase patterning is an important point of penetration to understand the ZF dynamics. However, it does not explicitly demonstrate how EP contributes to Θ_m's structure.

B. Particle contribution to zonal flow generation

The Taylor's identity provides a key relation that bridges the RF and the guiding center density fluxes of different particles[25]. To see this, we use the quasi-neutrality condition in the presence of EPs:

$$\delta n_{i,pol} + \delta n_{i,g} + \delta n_{EP} - \delta n_e = 0, \tag{3}$$

where $\delta n_{i,pol}$ is ion's polarization density and $\delta n_{i,g}$ is ion's guiding center density. Due to the smallness of the electron's gyro-radius, its polarization density is ignorable, i.e., $\delta n_e = \delta n_{e,g}$. Also, for convenience, we have assumed the EP has the same charge with the ion, $q_{EP} = q_i = e$. The ion's (or EP's) polarization density has a general form of $\delta n_{pol} = -n_0(1-\Gamma_0(b))e\tilde{\phi}/T$, where $\Gamma_0(b) = I_0(b)\mathrm{e}^{-b}$ with I_0 the modified Bessel function of the zeroth kind[26]. In ITG turbulence, for ions, one has $b = b_i = k_\perp^2\rho_{ti}^2 < 1$ and using Padé's expansion, $\delta n_{i,pol}$ can be approximated as $\delta n_{i,pol} \cong -\chi_i k_\perp^2\rho_{ti}^2 e\tilde{\phi}/T_i$ with $\chi_i = 1/(1+k_\perp^2\rho_{ti}^2)$ the polarization rate. χ_i varies with different $k_\perp$s and for analytical convenience, we use a statistically averaged

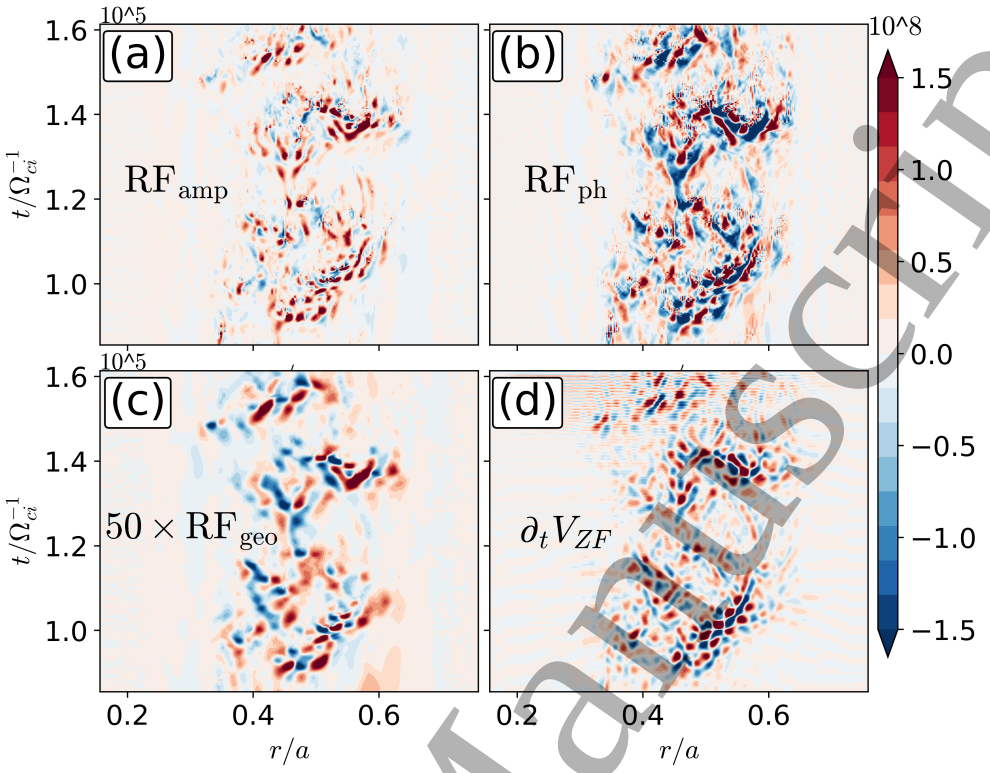

FIG. 2. Reynolds' force from: (a) turbulence inhomogeneity $\mathrm{RF}_{\mathrm{amp}}$, (b) phase curvature $\mathrm{RF}_{\mathrm{ph}}$ and (c) geometric effect $\mathrm{RF}_{\mathrm{geo}}$. (d) Spatiotemporal profile of ZF generation rate.

$\chi_{i,eff} = 1/(1 + k_{\perp,c}^2\rho_{ti}^2)$ instead of the $\chi_i(k_\perp)$, with $k_{\perp,c}$ the characteristic wave number of the ITG turbulence and typically $\chi_{i,eff} \simeq 0.5$ (or $k_{\perp,c}^2\rho_{ti}^2 \simeq 1$). With $-k_\perp^2\rho_{ti}^2 \Rightarrow \rho_{ti}^2\nabla_\perp^2$, Eq. (3) can be recast into a Poisson equation:

$$\rho_{ti}^2\nabla_\perp^2\frac{e\tilde{\phi}}{T_i} = -\frac{1}{\chi_{i,eff}}\frac{\delta n_{i,g} + \delta n_{EP} - \delta n_e}{n_{i,0}}. \tag{4}$$

The non-triviality of the EP effect can be glimpsed from: (1) $\delta n_{i,g} - \delta n_e$ could be comparable with δn_{EP}, even though $|\delta n_{EP}| \ll |\delta n_{i,g}|, |\delta n_e|$; (2) the ZF generation is a multi-scale problem, though at meso-scale (a few ρ_{ti}s), the collective dynamics of ions and electrons are important, the EP dynamics potentially plays a more important role at macro-scale (a few $\rho_{t,EP}$s) and hence it may stimulate the ITG-ZF coupling at macro-scale, which is inactive in the absence of EPs. Similar to ions, for EPs, we have $\delta n_{EP} = \delta n_{EP,pol} + \delta n_{EP,g}$. For $\delta n_{EP,pol}$, it is $b = b_{EP} = k_\perp^2\rho_{t,EP}^2 \gg 1$ and $\Gamma_0(b_{EP})$ is then approximated as $\Gamma_0(b_{EP}) \propto 1/\sqrt{b_{EP}} \ll 1$. Therefore, $\delta n_{EP,pol}$ will be dominated by adiabatic response, i.e., $\delta n_{EP,pol} \simeq -n_{EP,0}e\tilde{\phi}/T_{EP}$ and its contribution to the particle flux is ignorable. Hence, we have $\Gamma_{EP} = \langle\delta n_{EP}\tilde{v}_r\rangle \simeq \langle\delta n_{EP,g}\tilde{v}_r\rangle = \Gamma_{EP,g}$. This is in essence the conventional wisdom that the direct coupling of EP to ITG is weak because the EP's gyro-radius significantly exceeds the wavelength of the ITG mode. However, it should be noticed that there is no pre-judgement that the response of EP guiding center density to ITG is ignorable. Its role in macro-scale ZF generation will

be disclosed here. To verify this speculation, we inspect the contributions of each term on the RHS of Eq. (4) to the Reynolds' force.

According to the Taylor's identity, the RF is equal to the vorticity flux: $\mathrm{RF} = \left\langle \nabla_\perp^2 \tilde{\phi}\tilde{v}_r \right\rangle / B_0$. Using Eq. (4), this relation is re-expressed as

$$\mathrm{RF} = \frac{\Omega_{ci}}{\chi_{i,eff} n_{i,0}} (\Gamma_{i,g} - \Gamma_e + \Gamma_{EP,g}), \tag{5}$$

with $\Gamma_{i,g} = \langle \delta n_{i,g} \tilde{v}_r \rangle$ the guiding center flux of the ions and $\Gamma_e = \langle \delta n_e \tilde{v}_r \rangle$ the electron particle flux. The fluxes on the RHS of Eq. (5) reflect the degree of coherent coupling between each type of particles with the ITG velocity fluctuations. From a mechanical perspective, the RHS of Eq. (5) represents a radial currents produced by guiding centers of background plasmas and the EPs, and hence it is proportional to the $J \times B$ force in the poloidal direction that drives the ZF[27].

C. Cross-phase Coherence and Macro-scale Zonal Flow Formation

Eq. (5) provides a straightforward way for assessing the contributions of different species to the total RF. The RF associated with $(\Gamma_{i,g} - \Gamma_e)$ is plotted in Fig. 3(a). As can be seen, it is dominated by meso-scale structures. Fig. 3(b) shows that $\Gamma_{EP,g}$ is mainly at macro-scale and its amplitude is comparable with $(\Gamma_{i,g} - \Gamma_e)$, though $|\delta n_{EP,g}| \ll |\delta n_{i,g}|, |\delta n_e|$(Fig. 3(c)). A further inspection reveals that this is due to the phase coupling effect between $\delta n_{EP,g}$ and δv_r, with the cross-phase $\Theta_{EP,v_r} = \Theta_{EP} - \Theta_{v_r}$ and $\delta n_{EP,g} = |\delta n_{EP,g}| e^{i\Theta_{EP}}$ and $\tilde{v}_r = |\tilde{v}_r| e^{i\Theta_{v_r}}$. Fig. 3(d-f) shows that the averaged cosines of the EP cross-phase $\langle \cos(\Theta_{EP,v_r}) \rangle$ significantly exceed those of ion's $\langle \cos(\Theta_{i,v_r}) \rangle$ and electron's $\langle \cos(\Theta_{e,v_r}) \rangle$, indicating the strong phase coherence between EP and the ITG fluctuations. By checking the spatiotemporal evolutions of the three cosine values (Fig. 3(g-i)), it finds that Θ_{EP,v_r} tends to form a 'shock layer' pattern in its linear stage[28–30] and interestingly, this pattern persists into its nonlinear stage. Similarly, the ions and electrons also exhibit phase resilience in their nonlinear stage. The difference is that their cross-phases with v_r are locked to an incoherent state, which means the density perturbations and radial velocities of particles become out of phase in such a way that their combined effect results in negligible net particle and charge flux, hence reducing their ZF driving.

The cross-phase dynamics rely on the kinetic response of different particles to the ITG fluctuations. We plot the contours of their perturbed guiding center distributions $\delta F_{j,g}(v_\parallel, v_\perp)$ with $j = i, e, EP$. As shown in Fig. 4, the cross-phases at the maxima of $|\delta F_{i,g}|$ and $|\delta F_{e,g}|$ are $\pi/2$ and $-\pi/2$, respectively. It is notable to observe that $|\delta F_{EP,g}|$ reaches its maximum at a relatively low energy, $\sim 0.1 T_{EP} \sim 2T_i$, with a corresponding cross-phase $\Theta_{F_{EP},v_r} \sim \pm\pi$. In other words, the low energy component of the EP tends to produce a large amplitude response, which is also consistent with previous work[31]. Fig. 4(c) also shows that most active EPs are deeply trapped.

To obtain analytically the kinetic response of EP to the ITG, first note that the perturbed

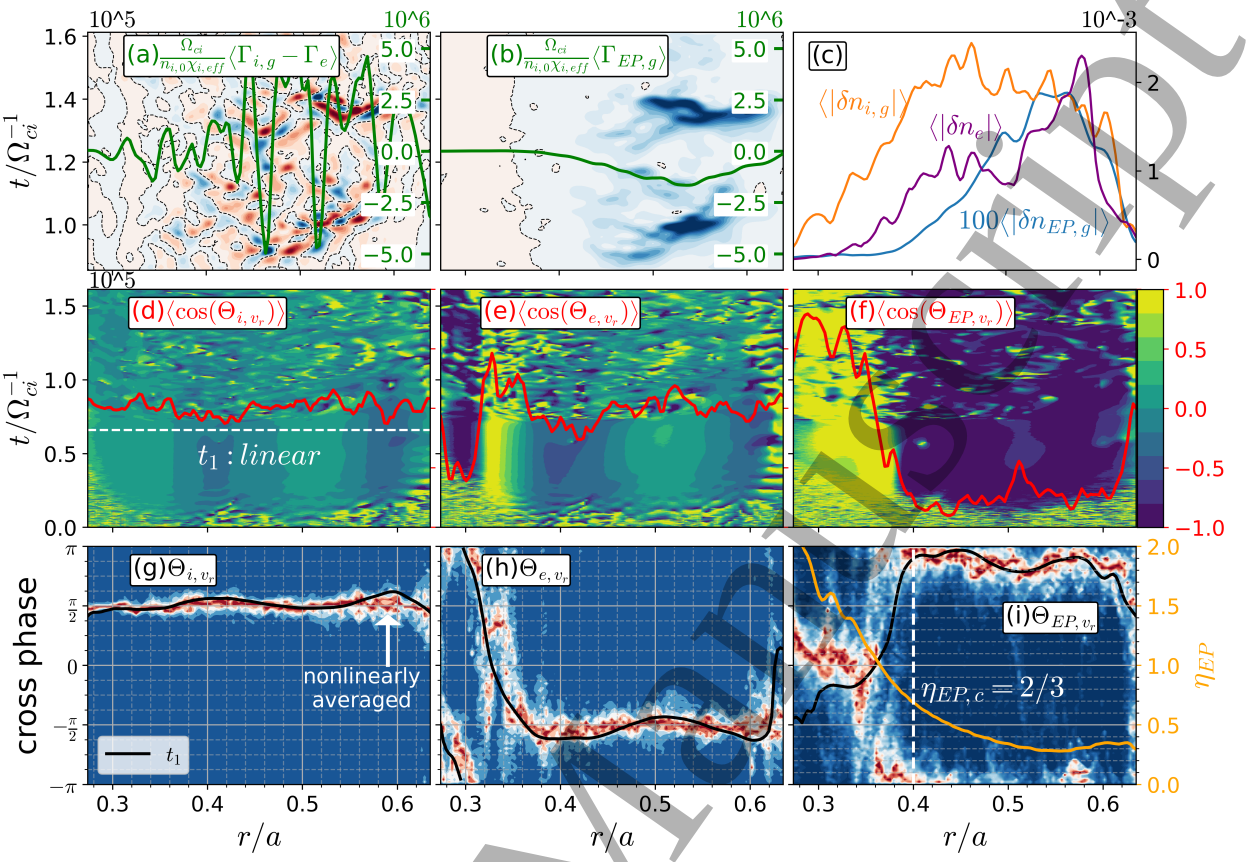

FIG. 3. Spatiotemporal pattern of the Reynolds' force (contours) and its averaged values (green lines) (a) for ions and electrons, and (b) for the EPs. (c) The averaged guiding center densities. (d)-(f) Spatiotemporal patterns (contours) of the cosines of three cross-phases and their averaged values (red lines). (g)-(i) The three cross-phases in their linear stage (black) and nonlinear stage (contour). Data in (c)-(i) is from the most unstable ITG mode with $m = 48$ and $n = 16$.

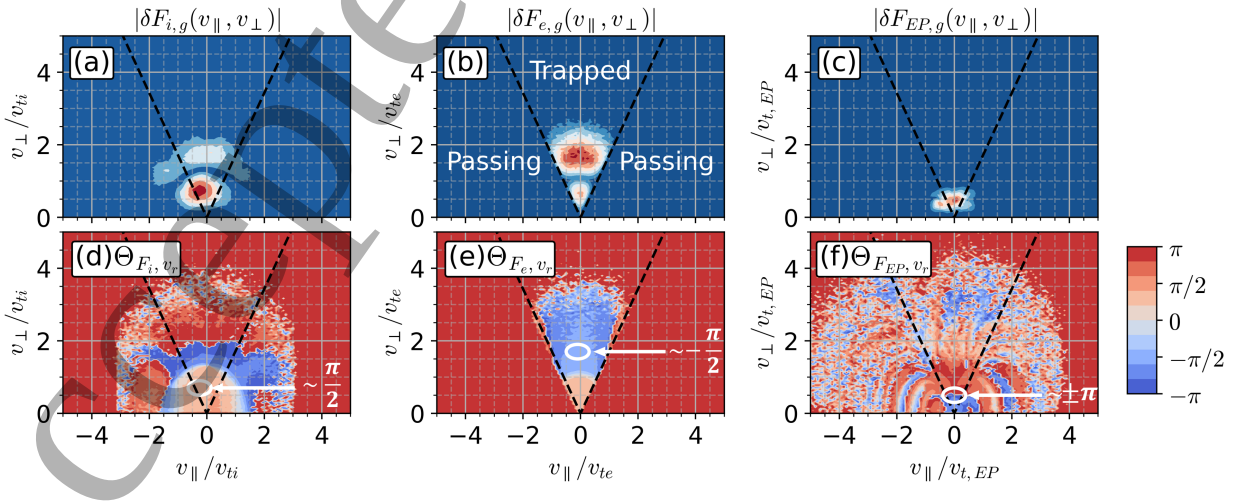

FIG. 4. Contours of the amplitudes ((a)-(c)) and the cross-phases ((d)-(f)) of $\delta F_{i,g}$, $\delta F_{e,g}$ and $\delta F_{EP,g}$ at $r = 0.46a$.

guiding center distribution function of the EP $\delta f_{EP,g}$ has a form of:

$$\delta f_{EP,g} = \delta h_{EP} - f_{0EP} J_{0EP} \frac{e\phi}{T_{EP}}, \tag{6}$$

where $J_{0EP} \equiv J_0(k_\perp \rho_{EP})$, J_0 is the Bessel function of the zeroth kind. For trapped EPs, δh_{EP} is determined by the bounce averaged equation[32]:

$$(\omega - \langle \omega_{D,EP} \rangle_b) \delta h_{EP} = J_{0EP} \frac{e \langle \phi \rangle_b}{T_{EP}} f_{0EP} (\omega - \omega^T_{*,EP}), \tag{7}$$

where $\langle \phi \rangle_b$ is the bounce averaged potential, $\omega^T_{*EP} = \omega_{*EP} [1 + \eta_{EP} (E/T_{EP} - 3/2)]$ is EP's diamagnetic frequency, with $\omega_{*EP} = k_\theta T_{EP}/(eB_0 L_{n,EP})$, $L_{n,EP} = -(\partial_r \ln n_{EP})^{-1}$, $L_{T,EP} = -(\partial_r \ln T_{EP})^{-1}$, $\eta_{EP} = L_{n,EP}/L_{T,EP}$ and k_θ is the poloidal wave number. $\langle \omega_{D,EP} \rangle_b$ is trapped EP's toroidal precession frequency and it has a form of:

$$\langle \omega_{D,EP} \rangle_b = \omega_{*EP} \frac{L_{n,EP}}{R} \frac{E}{T_{EP}} G(\hat{s}, \kappa), \tag{8}$$

with R the major radius of a tokamak, $E = m_{EP} v^2/2$ the particle energy, $\hat{s} = \mathrm{d} \ln q / \mathrm{d} r$ the magnetic shear, $\kappa = (1 - \mu B_{min}/E)/[(B_{max} - B_{min})/B_{max}]$ where $\mu = m_{EP} v_\perp^2/2B$ is the magnetic moment and B_{max}, B_{min} are the maximum and minimum of $|B|$ that a particle experiences during its unperturbed orbit excursion, respectively. $G(\hat{s}, \kappa) = 2E(\kappa^2)/K(\kappa^2) - 1 + 4\hat{s}(E(\kappa^2)/K(\kappa^2) + \kappa^2 - 1)$, $E(\kappa^2)$ and $K(\kappa^2)$ are the complete elliptic integral of the first and the second kind, respectively. For deeply trapped particles ($|v_\parallel| \ll |v_\perp|$ and $v_\perp^2 \simeq v^2$), one has $\kappa \ll 1$ and $G(\hat{s}, \kappa) \simeq 1$, thus $\langle \omega_{D,EP} \rangle_b$ can be simplified as $\langle \omega_{D,EP} \rangle_b = \omega_{*EP}(L_{n,EP}/R)[v^2/(2v^2_{t,EP})]$, and, neglecting the mode amplitude variation along the field lines, the bounce-averaged potential $\langle \phi \rangle_b$ can be approximated as ϕ. As the frequency of ITG mode ω_{ITG} is on the order of ion diamagnetic frequency $k_\theta T_i/(eB_0 L_{ni})$, the RHS of Eq. (7) is dominated by ω^T_{*EP} term provided that $\omega_{ITG}/\omega_{*EP} \sim (T_i/T_{EP})(L_{n,EP}/L_{ni}) \ll 1$. This constraint limits our analysis to a parameter regime where $L_{n,EP}/L_{ni} \ll T_{EP}/T_i$, a condition that is easily met as $T_{EP}/T_i \gg 1$. Then Eq. (7) can be simplified as:

$$\delta h_{EP} = J_{0EP} \frac{e\phi}{T_{EP}} F_{0EP} \frac{-\omega^T_{*,EP}}{\omega - \langle \omega_{D,EP} \rangle_b}. \tag{9}$$

Substituting Eq. (9) into Eq. (6) and integrating over the velocity space, one arrives at:

$$\frac{\delta n_{EP,g}}{n_{EP,0}} = -\frac{e\tilde{\phi}}{T_{EP}} \left[\Gamma_0(b_{EP}) + \left\langle \frac{\omega^T_{*EP} J_0^2 f_{0EP}}{\omega - \langle \omega_{D,EP} \rangle_b} \right\rangle_v \right], \tag{10}$$

where $\langle \cdot \rangle_v \equiv \int \mathrm{d}^3 v$, $\omega^T_{*EP} = \omega_{*EP} \left[1 + \eta_{EP} \left(\frac{E}{T_{EP}} - \frac{3}{2} \right) \right]$ and $\omega_{*EP} = k_\theta T_{EP}/(eB_0 L_{n,EP})$ is EP's diamagnetic frequency, with $\eta_{EP} = L_{n,EP}/L_{T,EP}$, $L_{n,EP} = -(\partial_r \ln n_{EP})^{-1}$, and $L_{T,EP} = -(\partial_r \ln T_{EP})^{-1}$. $\langle \omega_{D,EP} \rangle_b$ is the toroidal precession frequency. $|\delta n_{EP,g}|$ is dominated by its resonant EPs: $\omega = \omega_{ITG} = \langle \omega_{D,EP} \rangle_b$, which corresponds to an energy

$\sim \frac{1}{2}m_{EP}v^2(\text{resonance}) = T_{EP}(\omega_{ITG}/\omega_{*EP})(R/L_{n,EP}) \ll T_{EP}$ as $|\omega_{ITG}| \ll |\omega_{*EP}|$ and $R/L_{n,EP} \simeq 1$. This is consistent with the distribution in Fig. 4(c). Near the resonant velocity, we have:

$$\frac{\mathrm{Im}(\delta n_{EP,g}/\tilde{\phi})}{\mathrm{Re}(\delta n_{EP,g}/\tilde{\phi})} \propto \frac{\omega_{*,EP}}{\gamma_{ITG}}(1-\frac{3}{2}\eta_{EP}), \tag{11}$$

which indicates that there exists a critical value $\eta_{EP,c} = 2/3$, across which the sign of the cross-phase between $\delta n_{EP,g}$ and $\tilde{\phi}$ (or $\tilde{v}_r$) flips sign. Since $\omega_{*,EP}/\gamma_{ITG} \gg 1$, the transition layer in the cross-phase profile would exhibit 'shock'-like structure, as shown in Fig. 3(i), with the 'downstream' and 'upstream' of the shock layer being locked to 0 and π, respectively. In short, even though the amplitude ($|\delta n_{EP,g}|$) of EP's response to the ITG is dominated by their low energy component, their cross-phase with the ITG (Θ_{EP,v_r}) is determined by the EPs at $T = T_{EP}$.

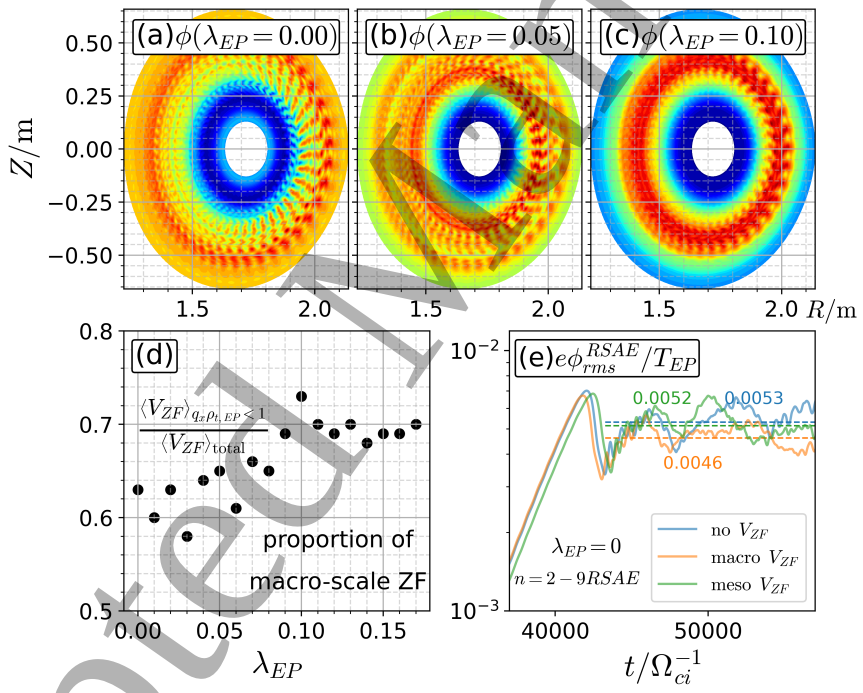

FIG. 5. (a)-(c)Distribution of ITG turbulence with zonal flow for different λ_{EP}s. (d) Relation between macro-scale ZF proportion and λ_{EP}. (e) Saturated RSAE levels for different types of ZFs.

Figure 5(a)-(c) shows that with the increase of the EP concentrations, the electrostatic potential tends to exhibit macroscopic patterns. This feature can be seen quantitatively by defining a macro-scale ZF ratio (Fig. 5(d)). The macro-scale ZF driven associated with the EPs would suppress macro-scale modes (i.e., RSAE in this configuration). To demonstrate the effect of the macro-scale ZF on the saturated levels of the RSAE at multi-modes state, we carry out a numerical experiment. First, we extract the time-averaged (over nonlinear stage) zonal flow from our ITG turbulence simulation, and decompose it into meso-scale and macro-scale pieces. Then, we impose these zonal flows into the nonlinear RSAE simulations,

and meanwhile exclude the self-generated zonal flows from the RSAE themselves. By comparing the RSAE saturation amplitudes with and without the imposed zonal flows, we can assess the effect of the ITG-generated zonal flow on RSAE saturation. Fig. 5 (e) shows that the saturated RSAE intensities are almost not changed for the ZF-free and meso-scale-only ZF cases. While for the macro-scale-only ZF scenario, the RSAE intensity is remarkably reduced. It is speculated that with the increase of λ_{EP}, the macro-scale modes will be suppressed more effectively. Thus, by simulating macro-scale ZF generation in ITG turbulence, the AE triggered EP loss can potentially be reduced, so that confinement of the EPs in the core region gets improved.

IV. CONCLUSION

In this work, we have investigated the direct role of EPs in stimulating macro-scale ZF generation within ITG turbulence through nonlinear gyrokinetic simulations. By introducing the concept of specific ZF capability, we find that the presence of EPs significantly enhances the efficiency of ZF production beyond their known linear stabilization effects.

A detailed analysis reveals that this enhancement originates from the strong in-phase coupling between the EP guiding center density and the ITG radial velocity fluctuation. This interaction leads to a substantial EP guiding center flux at macro-scale, which contributes to the Reynolds' force comparably with the thermal particles. The persistence of the cross-phase structure from linear to nonlinear stages underscores the robustness of this mechanism.

Furthermore, kinetic analysis shows that although the EP response is governed by resonant particles with lower energies, the in-phase coupling emerges because of EP's large diamagnetic frequency due to EP's high temperature. The resulting macro-scale ZF is found to be effective in suppressing macro-scale AEs, indicating a self-regulating mechanism that could improve EP confinement in burning plasmas.

These findings highlight a previously underappreciated nonlinear pathway through which EPs contribute to turbulence regulation and confinement improvement. This mechanism may offer new insights for the control of transport and stability in future fusion devices.

It should be noted that, to focus on the impact of EP on the ITG turbulence self-organization process, our current simulations only include EP, ITG and ZF, and not include electromagnetic instabilities such as AEs. Including self-consistent AE modeling is essential for a more complete understanding of the EP-AE-ITG-ZF system. Future work will focus on extending the current framework to incorporate these effects, aiming to provide a more self-consistent picture of multi-scale plasma turbulence and energetic particle dynamics.

The present analysis and simulations are conducted within the framework of the gyrokinetic equations. However, at reactor scale, the EP gyro-radius become even larger (e.g. $\rho_{Tf} \approx 5$cm for 3.4MeV alpha particles at $B = 5$T), which can induce more errors in the guiding center approximation. Particularly, the fusion reactor needs to operate at a time scale of thousand seconds and it would add more accumulative error. Thus, it is essential to validate and extend the present findings by carrying out full-f simulation.

ACKNOWLEDGMENTS

This work was supported by the National MCF energy R&D Program of China under Grant No. 2024YFE03270400.

[1] V. G. Kiptily, R. Dumont, M. Fitzgerald, *et al.*, Evidence of electron heating by alpha particles in jet deuterium-tritium plasmas, Phys. Rev. Lett. **131**, 075101 (2023).

[2] A. Bierwage, K. Shinohara, Y. O. Kazakov, *et al.*, Energy-selective confinement of fusion-born alpha particles during internal relaxations in a tokamak plasma, Nature Communications **13**, 3941 (2022).

[3] W. W. Heidbrink, Basic physics of Alfvén instabilities driven by energetic particles in toroidally confined plasmasa), Physics of Plasmas **15**, 055501 (2008).

[4] L. Chen, R. B. White, and M. N. Rosenbluth, Excitation of internal kink modes by trapped energetic beam ions, Phys. Rev. Lett. **52**, 1122 (1984).

[5] P. H. Diamond, S.-I. Itoh, K. Itoh, *et al.*, Zonal flows in plasma—a review, Plasma Physics and Controlled Fusion **47**, R35 (2005).

[6] D. Kim, S. Park, G. Choi, *et al.*, Turbulence stabilization in tokamak plasmas with high population of fast ions, Nuclear Fusion **63**, 124001 (2023).

[7] G. Wilkie, A. Iantchenko, I. Abel, *et al.*, First principles of modelling the stabilization of microturbulence by fast ions, Nuclear Fusion **58**, 082024 (2018).

[8] A. D. Siena, T. Görler, H. Doerk, *et al.*, Fast-ion stabilization of tokamak plasma turbulence, Nuclear Fusion **58**, 054002 (2018).

[9] A. Di Siena, T. Görler, E. Poli, *et al.*, Resonant interaction of energetic ions with bulk-ion plasma micro-turbulence, Physics of Plasmas **26**, 052504 (2019).

[10] N. Bonanomi, P. Mantica, A. Di Siena, *et al.*, Turbulent transport stabilization by icrh minority fast ions in low rotating jet ilw l-mode plasmas, Nuclear Fusion **58**, 056025 (2018).

[11] A. Di Siena, R. Bilato, T. Görler, *et al.*, New high-confinement regime with fast ions in the core of fusion plasmas, Phys. Rev. Lett. **127**, 025002 (2021).

[12] M. Romanelli, A. Zocco, F. Crisanti, *et al.*, Fast ion stabilization of the ion temperature gradient driven modes in the joint european torus hybrid-scenario plasmas: a trigger mechanism for internal transport barrier formation, Plasma Physics and Controlled Fusion **52**, 045007 (2010).

[13] J. Citrin, J. Garcia, T. Görler, *et al.*, Electromagnetic stabilization of tokamak microturbulence in a high-β regime, Plasma Physics and Controlled Fusion **57**, 014032 (2014).

[14] Y. Todo, H. Berk, and B. Breizman, Nonlinear magnetohydrodynamic effects on alfvén eigenmode evolution and zonal flow generation, Nuclear Fusion **50**, 084016 (2010).

[15] Z. Qiu, L. Chen, and F. Zonca, Effects of energetic particles on zonal flow generation by toroidal alfvén eigenmode, Physics of Plasmas **23**, 090702 (2016).

[16] A. D. Siena, T. Görler, E. Poli, *et al.*, Electromagnetic turbulence suppression by energetic particle driven modes, Nuclear Fusion **59**, 124001 (2019).

[17] G. Brochard, C. Liu, X. Wei, *et al.*, Saturation of fishbone instability through zonal flows

driven by energetic particle transport in tokamak plasmas, Nuclear Fusion **65**, 016052 (2025).

[18] G. Brochard, C. Liu, X. Wei, *et al.*, Saturation of fishbone instability by self-generated zonal flows in tokamak plasmas, Phys. Rev. Lett. **132**, 075101 (2024).

[19] J. Garcia, Y. Kazakov, R. Coelho, , *et al.*, Stable deuterium-tritium plasmas with improved confinement in the presence of energetic-ion instabilities, Nature Communications **15**, 7846 (2024).

[20] J. Ruiz Ruiz, J. Garcia, M. Barnes, *et al.* (the JET Contributors and the EUROfusion Tokamak Exploitation Team), Measurement of zero-frequency fluctuations generated by coupling between alfvén modes in the jet tokamak, Phys. Rev. Lett. **134**, 095103 (2025).

[21] J. Varela, C. Hidalgo, T. Tokuzawa, *et al.*, Generation of shear flows induced by ae / epm in lhd plasma, Nuclear Fusion **65**, 026002 (2024).

[22] X. Wei, P. Liu, G. Choi, *et al.*, Formulations and verification of gyrokinetic simulation of kinetic-mhd processes in toroidal plasmas (2025), arXiv:2109.08873 [physics.plasm-ph].

[23] S. Taimourzadeh, E. M. Bass, Y. Chen, *et al.*, Verification and validation of integrated simulation of energetic particles in fusion plasmas, Nuclear Fusion **59**, 066006 (2019).

[24] G. Tardini, J. Hobirk, V. Igochine, *et al.*, Thermal ions dilution and itg suppression in asdex upgrade ion itbs, Nuclear Fusion **47**, 280 (2007).

[25] G. I. Taylor and W. N. Shaw, I. eddy motion in the atmosphere, Philosophical Transactions of the Royal Society of London. Series A, Containing Papers of a Mathematical or Physical Character **215**, 1 (1915).

[26] D. H. E. Dubin, J. A. Krommes, C. Oberman, and W. W. Lee, Nonlinear gyrokinetic equations, The Physics of Fluids **26**, 3524 (1983).

[27] P. H. Diamond and Y. Kim, Theory of mean poloidal flow generation by turbulence, Physics of Fluids B: Plasma Physics **3**, 1626 (1991).

[28] Z. B. Guo and P. H. Diamond, Zonal flow patterns: How toroidal coupling induces phase jumps and shear layers, Phys. Rev. Lett. **117**, 125002 (2016).

[29] T. C. Xu, X. Y. Yang, Z. B. Guo, *et al.*, Observation of phase pattern accelerating zonal flow, Nuclear Fusion **60**, 016029 (2020).

[30] Y. Sarazin, G. Dif-Pradalier, X. Garbet, *et al.*, Key impact of phase dynamics and diamagnetic drive on reynolds stress in magnetic fusion plasmas, Plasma Physics and Controlled Fusion **63**, 064007 (2021).

[31] W. L. Zhang, Z. H. Lin, and L. Chen, Transport of energetic particles by microturbulence in magnetized plasmas, Phys. Rev. Lett. **101**, 095001 (2008).

[32] B. J. Kang and T. S. Hahm, Fast ion driven drift instability in reversed shear plasmas, Physics of Plasmas **26**, 042501 (2019).